BULLETIN OF THE EARTHQUAKE
RESEARCH INSTITUTE
Vol. 48 (1970), pp. 835-869

45. *Tsunami Source, Energy and the Directivity of Wave Radiation.*

By Kinjiro KAJIURA,

Earthquake Research Institute.

(Read June 23, 1970.—Received July 31, 1970.)

Abstract

Based on the long wave approximation, a formula to compute the tsunami wave form on a flat bottom generated by a broad crustal deformation is introduced. The energy transfer from the sea bottom to the water is examined in relation to the duration of the bottom movement. If the duration is less than several minutes, the deformation may be considered to be abrupt as far as the tsunami is concerned. However, if the movement is completed in a few second, the energy transferred to the compressional water waves might be larger than the tsunami energy.

The two-dimensional propagation of tsunami generated by a simple source of rectangular shape is explained by the superposition of various elementary waves. If the deformation of the bottom is a simple uplift or depression, the wave decay with distance near the source deviates from that due to geometrical spreading from a point source: in the direction of the major axis, the decay is faster, indicating a strong effect of diffraction, and in the direction of the minor axis, the decay is slower, indicating the approach to the one dimensional propagation. The variation of the directivity coefficient is conspicuous only for azimuths less than $\pi/4$ from the direction of the minor axis.

For long distances from the source, the directivity of energy radiation is proportional to the square of the lateral dimension of the source with respect to the direction of the observing point. The non-dispersive and dispersive wave forms are compared for long distances from the source, and it is concluded that the long wave approximation may be applicable for $p_a \gtrsim 4$, p_a being a parameter related to the dimension of the source, distance and the depth of water.

1. Introduction

The generating area of a large tsunami is elongated more and more as the magnitude of the earthquake increases, and the existence of the directivity of wave radiation from a tsunami source has been recognized

for a long time. For the causes of the directivity, the following two factors are considered to be most important: 1) the effect of the shape of a source, 2) the effect of the bottom topography in the vicinity of the source. Field evidences for the directivity of tsunamis were presented by Miyoshi (1955) and Hatori (1963).

As to the shape factor, several studies were undertaken both experimentally (Takahasi and Hatori, 1962) and theoretically (Momoi, 1962, 1963; Kajiura, 1963). As to the topographic factor, Miyoshi (1968) proposed a simple theory based on wave refraction. Recent numerical experiments by Aida (1969) for the Niigata tsunami revealed clearly the importance of these two factors in the consideration of tsunami propagation.

In spite of the importance of the directivity of energy radiation of a tsunami, adequate consideration has not been paid to this effect in the estimation of the total tsunami energy by a conventional method. If various errors in the estimation of tsunami energy are taken into account, the uncertainty of the estimated energy may amount to a factor of 10 for extreme cases. If the magnitude scale of the tsunami is to be defined in relation to the tsunami energy, more accurate determinations of tsunami energy seem to be essential (Soloviev, 1969).

Here, a problem arises as to the attenuation of the wave height with distance. The region of tsunami generation is mostly on the periphery of the ocean, and the nearest coast which is most severely affected by a large tsunami is located in the distance comparable to the dimension of the tsunami source. In this region, therefore, the propagation characteristics of the tsunami would be like the one-dimensional one. For a moderately long distance, R, from the source the attenuation of the wave height may be approximated by $H_0/\sqrt{R}$, in accordance with the geometrical spreading if the gravity wave dispersion is negligible. However, the proportionality factor H_0 would be a function of the direction because of the directional difference of wave radiation. In the estimation of the attenuation characteristic of the wave height with distance from field data, this is one of the factors responsible for the large scatter of data points by a factor of 3 or so in the wave height *vs* distance graphs (Soloviev, 1965; Iida, 1966). In actual cases, the situation is further complicated by the wave guide effect of a continental shelf.

In the present paper, a simple case of tsunami generation on a flat bottom is examined theoretically based on the long wave approximation to shed some light on the wave propagation characteristics and the energy radiation pattern from an elongated tsunami source of a large scale. Although various studies of this kind were made in the past and con-

siderable knowledge has been accumulated, it seems worthwhile to discuss the problem from a unified standpoint.

At first, the effect of duration of the bottom movement on the total energy transferred to the water body is examined. Next, the radiation pattern of the wave energy together with the directional difference of wave height is discussed. Lastly, for long distances from the source, asymptotic wave forms are computed and the validity of the long wave approximation is discussed by comparing the non-dispersive wave form with the dispersive one.

2. Wave generation by the bottom deformation

The generation and propagation of a tsunami in the sea of constant depth under various source conditions were already discussed by the author (Kajiura, 1963, hereafter referred to as Paper I). We consider now the wave directivity for a tsunami source of large dimensions under the linear long wave approximation. The limitation of the long wave approximation will be discussed in Section 7.

The linear wave equation for the tsunami generation is,

$$\nabla^2\zeta-\frac{1}{c^2}\frac{\partial^2\zeta}{\partial t^2}=-\frac{1}{c^2}\frac{\partial w_B}{\partial t}, \tag{2·1}$$

where ζ is the free surface elevation from the undisturbed level, $c^2=gh$ with g the acceleration due to gravity and h the constant depth of water. Here t is time, ∇^2 is the Laplacian operator in the horizontal co-ordinates, and w_B is the vertical velocity of the bottom movement, taken positively upwards.

A Green's function G in the infinite domain for the wave equation (2·1) is given by (see, for example, Morse and Feshbach, 1953),

$$G(\mathbf{r}, t \mid \mathbf{r}_0, t_0)=(2c/\sqrt{c^2(t-t_0)^2-(\mathbf{r}-\mathbf{r}_0)^2})H[c(t-t_0)-|\mathbf{r}-\mathbf{r}_0|], \tag{2·2}$$

where $\mathbf{r}$ is the position vector, the suffix 0 denotes quantities related to the source, and $H(x)$ is a unit step function with $H(x)=0$, for $x<0$, and $H(x)=1$, for $x>0$.

Making use of (2·2), the elevation ζ in the infinite domain can be written as,

$$\zeta(\mathbf{r}, t)=\frac{1}{4\pi c^2}\int_0^t dt_0\iint_S G(\mathbf{r}, t \mid \mathbf{r}_0, t_0)\frac{\partial w_B}{\partial t_0}ds_0, \tag{2·3}$$

where S covers the source area with ds_0 the surface element.

Now we assume that w_B is constant for a certain duration, $0\leqslant t\leqslant T$,

and zero otherwise and the total bottom deformation is $D(\mathbf{r}_0)$.
Then, it follows:

$$\partial w_B/\partial t_0=(D/T)\{\delta(0)-\delta(T)\}, \tag{2·4}$$

where $\delta(x)$ is Dirac's delta function.

Substituting (2·4) into (2·3) and taking the origin of the co-ordinates at the observing point, we have

$$\zeta=(\eta_1-\eta_2)/(2\pi cT), \tag{2·5}$$

where

$$\eta_i=\iint_S (D/\sqrt{\tau_i^2-r_0^2})H[\tau_i-r_0]ds_0, \tag{2·6}$$

and

$$\tau_1=ct, \quad \tau_2=c(t-T).$$

In the later discussion, we omit subscripts 0 for the source and i for η_i and τ_i for simplicity, unless otherwise noted.

In the polar co-ordinates (r, θ), we may write (2·6) in the form

$$\eta=\int_{r_1}^{r_2}(\Theta r/\sqrt{\tau^2-r^2})H[\tau-r]dr, \tag{2·7}$$

where

$$\Theta=\int_{\theta_1}^{\theta_2}D(\theta, r)d\theta. \tag{2·8}$$

In (2·7) and (2·8), the integral is limited within the source region so that the integral limits, $(r_1\cdot r_2)$ and $(\theta_1\cdot\theta_2)$ are determined by the geometry of the source. Here we may call $r\Theta$ as a directive source function relative to the observing point.

For a limiting case when $T\to 0$, we may transform (2·5) together with (2·7) into

$$\zeta=1/(2\pi)\partial\eta/\partial\tau=1/(2\pi)\left(\Theta(0)\delta(r_1)+\int_{r_1}^{r_2}\frac{\tau}{\sqrt{\tau^2-r^2}}\frac{\partial\Theta}{\partial r}H[\tau-r]dr\right). \tag{2·9}$$

If the observing point is in the source region $(r_1=0)$, $\Theta(0)$ in the right hand side is preserved.

If the source region (source dimension, L) is very far from the observing point (distance to the center of the source, R), namely $L/R\ll 1$, we may approximate, by taking the rectangular co-ordinates with the x-axis in the direction of the source center,

$$\sqrt{\tau^2-r^2}\simeq\sqrt{2R}\sqrt{\tau-x}, \quad \text{for } \tau/R\simeq 1.$$

Therefore, (2·6) may be approximated by

$$\eta\simeq\frac{1}{\sqrt{2R}}\int_{x_1}^{x_2}\frac{W(x)}{\sqrt{\tau-x}}H[\tau-x]dx, \tag{2·10}$$

where

$$W(x)=\int_{y_1}^{y_2}D(x, y)dy\,. \tag{2·11}$$

The limits of integration (x_1, x_2), (y_1, y_2) in (2·10) and (2·11), respectively, are determined by the geometry of the source and (x_2-x_1), (y_2-y_1) are of the order L with $L/R\ll 1$. In this case the directive source function $r\Theta$ in (2·7) is replaced by $W(x)$. For a limiting case when $T\to 0$, we can derive in place of (2·9),

$$\zeta=\frac{1}{2\pi}\frac{1}{\sqrt{2R}}\int_{x_1}^{x_2}\frac{1}{\sqrt{\tau-x}}\frac{\partial W}{\partial x}H[\tau-x]dx. \tag{2·12}$$

It is remarked that the approximations (2·10) and (2·12) deteriorate for the proximity of $x=x_1$ or x_2 unless $W(x)$ approaches zero. Although the directive source function $r\Theta$ always approaches zero as $r\to r_1$ or r_2, the corresponding directive source function $W(x)$ does not necessarily exhibit this feature unless (y_1-y_2) approaches zero as $x\to x_1$ or x_2.

For a simple geometry of the source, the directive source function can be expressed by an analytical formula and the generated wave form can be computed easily either analytically or numerically. Source models used in the present paper are:

Model A Rectangular shape with uniform (A1) or linear variation (A2) of the bottom deformation,

Model B Elliptic shape with uniform (B1), elliptic (B2), or parabolic (B3) deformation of the bottom,

Model C Circular shape with the uniform bottom deformation.

Model C is a special case of Model B and widely used for the study of the tsunami generation problem in the past.

3. Computation of wave forms for rectangular models

To compute the wave form due to an uniform deformation (Model A1) or due to a linear variation of the deformation (Model A2) in a rectangular area of the bottom, it is convenient to make use of the method of superposition. An elementary solution can be taken in various

way, but, here, we take an elementary source geometry as shown in Fig. 1. The origin of the co-ordinate is at the observing point, and the nearest corner of the source, P, is at (d, φ) or (x_p, y_p) with the source region in $x_p \leqslant x < \infty$ and $y_p \leqslant y < \infty$.

a) **Uniform deformation D_0**

In Fig. 1, we divide the source into two regions (1) and (2), and denote the solutions given by (2·7) as $\eta^{(1)}$ and $\eta^{(2)}$ for the regions (1) and (2), respectively. Then, $\eta^{(2)}$ can be obtained from $\eta^{(1)}$ by replacing φ by $\pi/2-\varphi$, or exchanging x_p and y_p. Let us now write the combination of $\eta^{(1)}$ and $\eta^{(2)}$ as $\eta(\tau/x_p, y_p)$, namely,

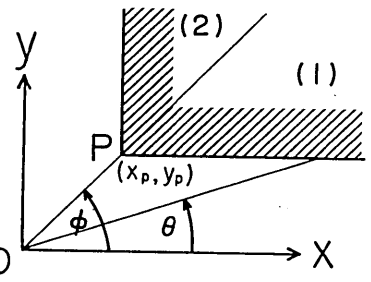

Fig. 1. Co-ordinate systems relative to the source geometry.

$$\eta(\tau/x_p, y_p)=\eta^{(1)}+\eta^{(2)}, \quad \text{for} \quad x_p, y_p \geqslant 0. \tag{3·1}$$

For the region (1), the directive source function can be written as

$$r\Theta = D_0 r\{\varphi - Sin^{-1}(y_p/r)\}H(r-d), \tag{3·2}$$

where r is the radial distance, and $H(r-d)$ is a unit step function.

Substituting (3·2) into (2·7), and performing the partial integration, we have

$$\eta^{(1)}/D_0 = \int_d^\tau \frac{\sqrt{\tau^2-r^2}}{\sqrt{1-(y_p/r)^2}} \frac{y_p}{r^2} dr, \quad \text{for} \quad \tau \geqslant d. \tag{3·3}$$

(3·3) can be transformed into:

$$\eta^{(1)} D_0 = \{\tau I(\tau/d, y_p) - y_p J(\tau/d, y_p)\}H(\tau-d), \tag{3·4}$$

where

$$\begin{aligned} I(\tau/d, y_p) &= \int_d^\tau \frac{y_p/r^2}{\sqrt{1-(r/\tau)^2}\sqrt{1-(y_p/r)^2}} dr \\ &= Sin^{-1}\{(y_p/d)\sqrt{(\tau^2-d^2)/(\tau^2-y_p^2)}\}, \end{aligned} \tag{3·5}$$

and

$$\begin{aligned} J(\tau/d, y_p) &= \int_d^\tau 1/\{\sqrt{1-(r/\tau)^2}\sqrt{1-(y_p/r)^2}\cdot\tau\} dr \\ &= Sin^{-1}\sqrt{(\tau^2-d^2)/(\tau^2-y_p^2)}. \end{aligned} \tag{3·6}$$

If the apex P is in the second quadrant, we have

$$\eta(\tau \mid x_p, y_p) = 2\eta(\tau \mid 0, y_p) - \eta(\tau \mid \mid x_p \mid, y_p)\,, \quad \text{for} \quad x_p<0\,, \quad y_p>0\,, \tag{3·7}$$

where

$$\eta(\tau \mid 0, y_p) = (\pi/2)(\tau - y_p)H(\tau - y_p)\,. \tag{3·8}$$

If the apex P is in the fourth quadrant, the solution is given by exchanging x_p and y_p in (3·7), and if the apex P is in the third quadrant, we have

$$\eta(\tau \mid x_p, y_p) = 2\eta(\tau \mid x_p, 0) - \eta(\tau \mid x_p, \mid y_p \mid)\,, \quad \text{for} \quad x_p<0,\ y_p<0\,. \tag{3·9}$$

Thus, the solution η for a rectangular source in a general position (the co-ordinates of 4 corners are (x_1, y_1), (x_2, y_1), (x_2, y_2), (x_1, y_2) with $(x_2>x_1,\ y_2>y_1)$ can be expressed by,

$$\eta(\tau) = \eta(\tau \mid x_1, y_1) + \eta(\tau \mid x_2, y_2) - \eta(\tau \mid x_1, y_2) - \eta(\tau \mid x_2, y_1)\,. \tag{3·10}$$

The wave form $\zeta(\tau)$ can be given by (5).

For the case of the instantaneous deformation, the wave form for the region (1) is derived directly from (2·9) as

$$\zeta^{(1)}/D_0 = I(\tau \mid d, y_p)H(\tau - d)/(2\pi)\,, \tag{3·11}$$

and the resultant solution $\zeta(\tau \mid x_p, y_p)$ can be constructed as in the case of $\eta(\tau \mid x_p, y_p)$.

b) **Linear variation of deformation**

The linear variation of deformation is given by $D=\alpha(x-\beta)$ in the region shown in Fig. 1. In this case, the contribution of the constant part $(-\alpha\beta)$ is the same as in the case of an uniform deformation provided that D is now put $(-\alpha\beta)$. For the linearly varying part, the directive source function is given by

$$r\Theta = r\int_{\theta_1}^{\theta_2} \alpha r \cos\theta\, d\theta\,, \tag{3·12}$$

where $x=r\cos\theta$, θ_1 and θ_2 are defined by $\sin\theta_1=y_p/r$ and $\cos\theta_2=x_p/r$. The integration gives

$$\Theta = \alpha(\sqrt{r^2-x_p^2} - y_p)\,, \tag{3·13}$$

and

$$d\Theta/dr = \alpha r/\sqrt{r^2-x_p^2}\,. \tag{3·14}$$

Substituting (3·13) into (2·7) and performing a partial integration, it follows:

$$\eta(\tau \mid x_p, y_p)=\alpha\int_d^\tau r\sqrt{\tau^2-r^2}/\sqrt{r^2-x_p^2}\,dr$$
$$=(\alpha/2)\{(\tau^2-x_p^2)J(\tau \mid d, x_p)-\sqrt{(\tau^2-d^2)(d^2-x_p^2)}\}H(\tau-d), \qquad (3\cdot15)$$

where $d^2=x_p^2+y_p^2$, and $J(\tau \mid d, x_p)$ is given by (3·6).

If the apex P is in the second quadrant, the solution is

$$\eta(\tau \mid x_p, y_p)=\eta(\tau \mid \mid x_p \mid, y_p), \quad \text{for} \quad x_p<0,\ y_p>0, \qquad (3\cdot16)$$

because of the antisymmetric character of the deformation with respect to the y-axis. The solution for the apex P in the fourth quadrant is given by

$$\eta(\tau \mid x_p, y_p)=2\eta(\tau \mid x_p, 0)-\eta(\tau \mid x_p, \mid y_p \mid),$$
$$\text{for} \quad x_p>0,\ y_p<0. \qquad (3\cdot17)$$

If P is in the third quadrant, we may write

$$\eta(\tau \mid x_p, y_p)=\eta(\tau \mid \mid x_p \mid, y_p) \quad \text{for} \quad x_p<0,\ y_p<0. \qquad (3\cdot18)$$

For the case of the sudden deformation ($T\to0$), the substitution of (3·14) into (2·9) gives

$$\zeta(\tau \mid x_p, y_p)=(\alpha\tau)/(2\pi)\int_d^\tau r/\sqrt{(\tau^2-r^2)(r^2-x_p^2)}\,dr$$
$$=(\alpha\tau)/(2\pi)J(\tau \mid d, x_p)H(\tau-d), \qquad (3\cdot19)$$

and the solution when P is not in the first quadrant is constructed similarly to the case of $\eta(\tau \mid x_p, y_p)$.

To compute the wave form due to the combination of the linear deformation of the bottom, we should superpose the solutions for each elementary part of the bottom deformation, which, in turn, can be expressed by the combination of elementary solutions given in this section.

4. Energy exchange associated with the bottom deformation between the solid bottom and the overlying water

a) Static energy and tsunami energy

The energy flux dE/dt to the overlying water by the vertical movement of the bottom can be computed from

$$dE/dt=\iint_S p_B w_B ds\,, \tag{4·1}$$

where p_B is the bottom pressure and S is the total area of the deformation.

The total flux of energy E_t to the water in the time interval $0\leqslant t\leqslant T$ is

$$E_t=\int_0^T\iint_S p_B w_B ds dt\,. \tag{4·2}$$

Now, under the long wave approximation, the pressure may be considered as hydrostatic:

$$p_B=\int_{\zeta_B}^{h+\zeta}\rho g dz=\rho g(h-\zeta_B+\zeta)\,, \tag{4·3}$$

where ρ is the density of the water, ζ and ζ_B are the vertical displacement of the water surface and the bottom, respectively. Substituting this pressure in (4·2), we may write,

$$E_t=E_S+E_D \tag{4·4}$$

where

$$E_S=\rho g\int_0^T\iint_S w_B(h-\zeta_B)dsdt\,, \tag{4·5}$$

and

$$E_D=\rho g\int_0^T\iint_S w_B\zeta ds dt\,. \tag{4·6}$$

Taking the relations $\partial\zeta_B/\partial t=w_B$, and $\zeta_B=D$ for $t\geqslant T$, into account, (4·5) is transformed into

$$E_S=\rho g\left(hV-\frac{1}{2}\iint_S D^2 ds\right), \tag{4·7}$$

where V is the total volume of the bottom deformation; $V=\iint Dds$.

The energy flux E_S is independent of the time characteristics of the tectonic movement and may be called the static energy exchange. If the total volume of the deformation is zero or negative, it is evident that E_S is negative, indicating the energy transmitted from the water column to the solid bottom. On the other hand, E_D depends on the time characteristics of the deformation and is always positive, so that we

may call E_D as the dynamic energy of a tsunami. This kind of separation of the energy exchange is originally envisaged by Miyoshi (1954) who proposed the concept of the efficiency of tsunami by defining the efficiency as E_D/E_S.

It is immediately clear in (4·6) that: 1) if the deformation is very slow (quasi-static), $\zeta \to 0$ and $E_D \to 0$, and 2) if the deformation is instantaneous, $\zeta \sim \zeta_B$ and $E_D = (1/2)\rho g \iint_S D^2 ds$. In case (2), the total energy transferred to the water is,

$$E_t = E_S + E_D = \rho g h V,$$

showing that E_t is equivalent to the potential energy to transfer the water mass ρV from the bottom to the surface. We denote the dynamic energy in the case (2) as E_{D0} and investigate the dependence of the ratio E_D/E_{D0} on the duration T of the bottom movement.

Taking (2·5) into account, we may write (4·6) in the form:

$$E_D = \rho g/(2\pi c T) \int_0^T \iint_S w_B \eta \, ds dt. \tag{4·8}$$

Therefore, E_D can be computed numerically, if η is found from (2·7) for $0 \leqslant t \leqslant T$. For a uniform circular model (Model C; diameter A, deformation D_0), a formula to compute η given by Takahasi (1942) is used

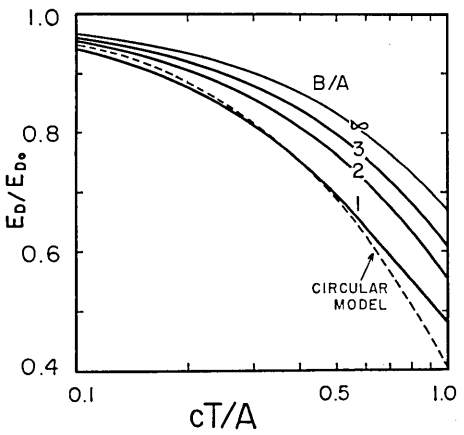

Fig. 2a. Efficiency of tsunami generation, E_D/E_{D0}, as a function of the duration of the bottom movement, cT/A, for Model A1.

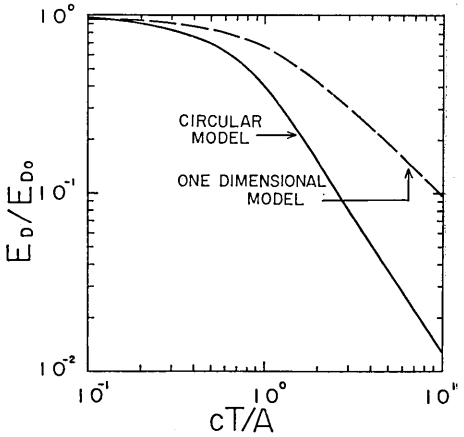

Fig. 2b. Efficiency of tsunami generation, E_D/E_{D0}, as a function of the duration of the bottom movement, cT/A, for one-dimensional and circular uniform source models.

(Eq. (36) in Takahasi's paper where ξ is used in place of η). For a uniform rectangular model (Model A1; side lengths A and B, deformation D_0), η is computed by the method given in § 3. For Model A1, $E_{D0}=(1/2)\rho g D_0^2 AB$ and for Model C, $E_{D0}=(1/8)\rho g D_0^2 \pi A$. A limiting case of $B\to\infty$ for a rectangular model corresponds to the one-dimensional case and the energy E_D for unit width can be derived easily (see Appendix A).

Fig. 2a shows the variation of E_D/E_{D0} with cT/A. It is seen that a rectangular model with $A=B$ is roughly similar to a circular model and with the increase of B, the variation of E_D/E_{D0} approaches that for an one dimensional model. In general, the decrease of E_D/E_0 is gradual for small values of cT/A. For large values of cT/A, the decrease of E_D/E_{D0} is proportional to $(cT/A)^{-n}$ with $n=1$ and 1.64 for the one dimensional and circular models, respectively, as shown in Fig. 2b.

b) Compressional wave energy and tsunami energy

In principle, if the bottom is uplifted ($w_B>0$), the energy is, at first, transferred from the solid earth to the overlying water by generating compressional waves in the water and then partly converted to gravity waves. To examine the relative importance of sound waves and gravity waves in terms of the generated wave energy, a simple model is considered, taking into account the fact that the gravity wave energy E_D can be approximated by E_{D0} for small values of $cT/A(\lesssim 0.2)$.

We confine the attention to the vertical direction only by assuming a very large horizontal dimension of the bottom uplift. If we assume $c/v\ll 1$ and $w_B/v\ll 1$, the sound pressure p^* at the bottom due to the bottom movement w_B is given by

$$p^*=\rho v w_B, \tag{4·9}$$

where the characteristic impedance of the sound wave is ρv with v the sound wave velocity. Therefore, the sound intensity I is,

$$I=p^* w_B=\rho v w_B^2, \tag{4·10}$$

and the total energy E_C transferred as sound in the time interval t is,

$$E_C=\rho w_B^2 v t. \tag{4·11}$$

The pressure change due to a reflected sound wave from the water surface interferes with the bottom after $t=2t_C$ where t_C is the travel time of the sound from the bottom to the free surface and

$$t_C=h/v. \tag{4·12}$$

Since this reflected wave is a rarefaction wave if the initial wave is a compressional one, the resultant bottom pressure is $p^*=-\rho v w_B$ and the transfer of energy takes place from water to the solid bottom as far as the sound wave is concerned, in the time interval $2t_C<t<4t_C$. After the termination of the bottom movement, the energy exchange between the solid earth and the water stops if the solid earth is perfectly rigid.

The time sequence of the sound pressure p^*, the variation of the free surface with both components of the sound wave and the hydrostatic displacement, the total sound energy E_C and the gravity wave energy E_D are shown in Fig. 3, where for the clarity of Fig. 3c, the hydrostatic energy is shown for a fictituous value of $c/v(=1/\sqrt{10})$. The variation of the free surface given in Fig. 3b is similar to the result obtained by Miyoshi (1959) in the general discussion of the generation of tsunamis in compressible water.

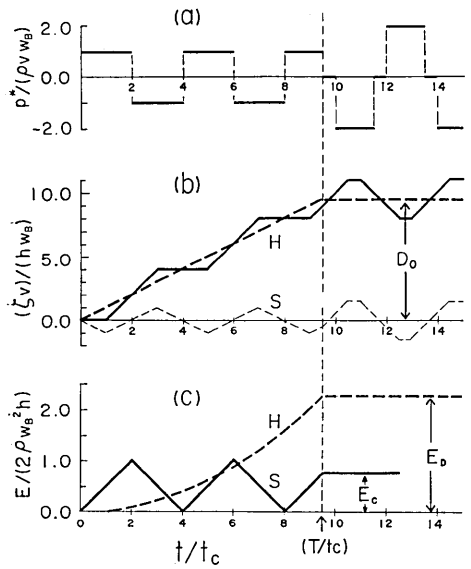

Fig. 3. a) Sound pressure variation p^* with time t/t_c at the bottom,
b) Surface disturbances ζ due to the hydrostatic displacement (H) and sound waves (S).
c) Variation of energy with time for both the hydrostatic displacement (H) and sound waves (S) in which $c/v=1/\sqrt{10}$ is assumed.

The energy E_C of the sound wave at the time of the termination of the bottom movement depends on the ratio T/t_C because E_C oscillates between 0 aud $E_{C\max}$ $(=2\rho w_B^2 h)$. On the other hand, the total energy E_D of a gravity wave generated by the bottom movement is

$$E_D=\rho g(w_B T)^2/2. \qquad (4\cdot13)$$

The ratio E_C/E_D can be given by

$$E_C/E_D=2v/(gT), \quad \text{for} \quad T\ll 2t_C \qquad (4\cdot14)$$

and

$$E_{C\,max}/E_D=4h/(gT^2) \quad \text{for} \quad T>2t_C. \qquad (4\cdot15)$$

The duration T_{crit}, for which the ratio E_{Cmax}/E_D becomes unity is

$$T_{crit}=2\sqrt{h/g}. \qquad (4\cdot16)$$

For a depth $h=2000$ m, T_{crit} is 28 sec. This value of T_{crit} indicates that, for the duration of several minutes of the bottom movement, the energy of the sound waves is negligible compared with gravity wave energy, and the opposite is true for a very short duration of the bottom movement.

It is very difficult to estimate the duration T of the bottom movement for actual earthquakes. From the study of the earthquake mechanism, the rupture velocity of an earthquake fault is considered to be of the order of S-wave velocity. If the fault length is, say, 400 km, and the rupture velocity 4 km/sec, the duration is 100 sec. In this model, the duration of the displacement at a particular location is assumed instantaneous and the displacement propagates along the fault. On the other hand, in the model adopted in the present paper, the displacement occurs in a broad area at the same time, but the vertical displacement is completed in the time interval T. Because of the difference of the models used, it is not possible to compare directly the duration T in the present paper with the duration of the fault movement considered in the study of the earthquake mechanism.

According to the study by Mikumo (1964) on atomospheric pressure waves generated by the tectonic deformation at the time of the Alaskan Earthquake of March 28, 1964, the deformation does not seem to have lasted much longer than 3 min. However, the lower limit of the duration could not be determined.

In view of the fact that the duration T of the seismic local source movement might be very small, the energy transfer to sound waves in the water due to the crustal deformation should be examined more carefully by taking the impedance of the crust into account.

5. Directivity of wave radiation for rectangular models (Model A)

The wave radiation due to the crustal deformation in a rectangular area of the bottom is discussed by using rectangular co-ordinates (x^*, y^*) and polar co-ordinates (R, θ) as shown in Fig. 4 with the origin at the center of a rectangle. The side lengths of the rectangle are A and B in the x^* and y^* directions, respectively. The time is measured from the first arrival of the wave disturbances at the observing point and is non-dimensional if we write $\tau^*=ct/A$. The method to compute ζ is already shown in

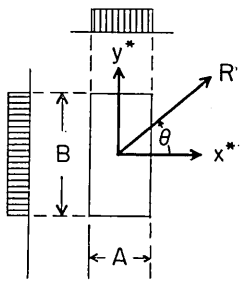

Fig. 4. Co-ordinate systems relative to the source geometry.

Section 3. The asymptotic solutions for long distances from the source are derived in Appendix B.

a) **Wave form due to an uniform bottom uplift (Model A1)**

In this model the vertical displacement of the bottom is D_0 with the duration T. Now consider the wave form travelling along the x^*-axis (see Fig. 4). It is easily understood that if the length B becomes infinite, the wave form would be similar to that of the one-dimensional case; that is to say, the wave form travels without change of shape. However, the effect of the finite length of B is felt as soon as the wave fronts originating from the side corners of the uplifted area arrive at the observing point. This sequence is shown in Fig. 5, for $B=3A$ and $cT/A=0.2$, where the distance x is measured from the edge of the source area; $x=x^*-A/2$. It is seen that, for $x/A=0$, the elevated portion of the wave form is the same as that for the one-dimensional model and the following depressed portion corresponds to the contribution from imaginary sources on both sides of the real source; namely, $D=-D_0$ for $|y^*|>B/2$, $|x^*|<A/2$.

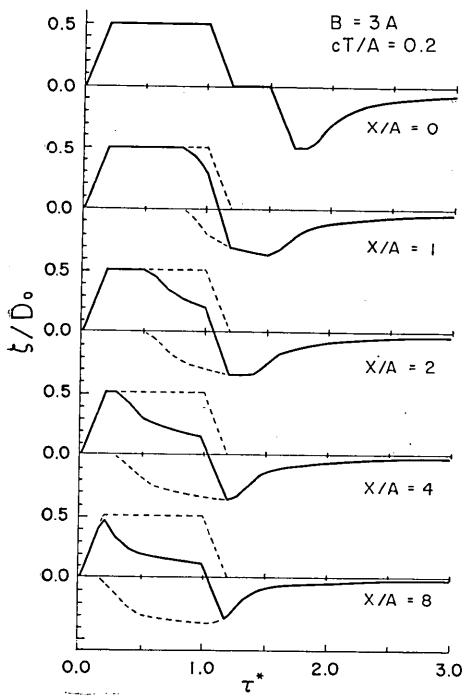

Fig. 5. Sequence of the variation of wave forms propagating in the direction of the x^*-axis, illustrating the effect of two-dimensionality of Model A1 with $cT/A=0.2$ and $B/A=3$.

With the increase of x/A, the depression wave due to imaginary sources begins to overlap that of the one-dimensional wave, the interval Δt of the arrival times of the two types of waves being given by $(\sqrt{x^2+(B/2)^2}-x)/c$. Therefore, the resultant wave form deviates more and more from the one-dimensional case. However, the maximum wave height does not change as long as $c\Delta t \geqslant T$.

The directional variations of wave forms for the case of $B/A=2$, $cT/A=0.2$, and $R/A=4$, are shown in Fig. 6. The variation of wave forms for $\theta=0$ to $\theta=\pi/2$ is very conspicuous, reflecting the variation of the directional source function. It may be noticed that for $\theta=0$ and

$\theta=\pi/2$, the wave forms are rather similar, provided that the total duration of the elevated portion of the wave is longer and the maximum height smaller for $\theta=\pi/2$ than for $\theta=0$. Judging from the shape of the directive source function, the main parts of the elevated portion and also the depressed portion in the wave forms for $\theta=0$ and $\theta=\pi/2$ become almost identical if we scale the distance R by the lateral dimension of the source area; namely, $R^*=R/B$ for $\theta=0$ and $R^*=R/A$ for $\theta=\pi/2$. The duration of the elevated portion of the wave form is roughly equal to the length of the source projected in the direction of the wave propagation. However, the wave form is very sensitive to the assumed source characteristics and the gravity wave dispersion, neglected in the present discussion, modifies the wave form drastically for long distances from the source (see § 7). It is then more advantageous to discuss the directivity of wave radiation in terms of energy than in terms of wave forms.

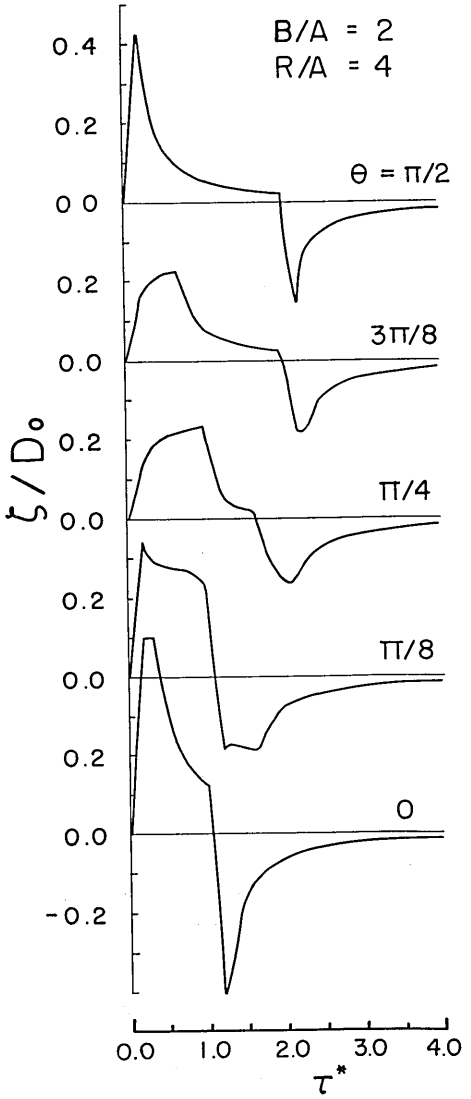

Fig. 6. Directional difference of wave forms at $R/A=4$, for Model $A1$ with $B/A=2$.

b) **Directivity of the energy radiation (Model A1)**

The total flux of gravity wave energy E_f for the unit width, transmitted in a particular direction may be computed approximately by the formula,

$$E_f=\rho g\int_0^\infty \zeta^2 c\,dt\,, \tag{5·1}$$

since the wave can be considered as progressive after leaving the source

area. The directively coefficient Q of the total wave energy flux at a distance R from the center of the wave source is defined by

$$Q=2\pi RE_f/E_D, \tag{5·2}$$

where E_D is the total energy of gravity waves. For a uniform bottom uplift in a rectangular area, E_D is already shown in Fig. 2a. The total energy flux E_f is computed numerically by (5.1) after evaluating ζ.

The dependence of Q on the distance $R^*(R/B$ for $\theta=0$, R/A for $\theta=\pi/2)$ is shown in Fig. 7 for $B/A=1$, 2, 3 and $\theta=0$, $\pi/2$. For large

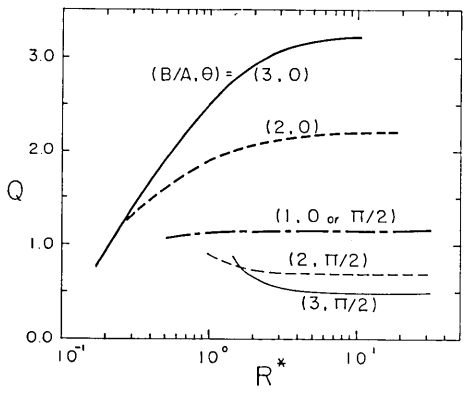

Fig. 7. Variation of the directivity coefficients $Q(0)$ and $Q(\pi/2)$ with the relative distance R^* ($R^*=R/B$ for $\theta=0$, and R/A for $\theta=\pi/2$) for Model $A1$ with $B/A=3$, 2, and 1, and $cT/A=0.2$.

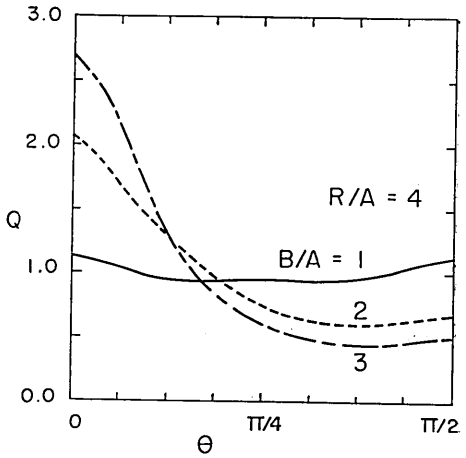

Fig. 8. Directivity coefficient at $R/A=4$ as a function of the azimuth θ for Model $A1$ with B/A=1, 2, 3, and $cT/A=0.2$.

values of R^*, Q becomes constant, but, for small values of R^*, Q decreases for $\theta=0$, and increases for $\theta=\pi/2$ with the decrease of R^* except for the case of $B/A=1$. This nature of Q reflects the following features of energy propagation. E_f decreases inversely proportional to R^* for $R^*\gtrsim 4$ but, for small values of R^*, the deviation from this law becomes significant as B/A increases. In particular, for $R^*\lesssim 1$ and $B/A\gtrsim 3$, the energy flux $E_f(0)$ (in the direction of the minor axis) does not vary much, indicating the approach of the wave form to the one-dimensional case. On the other hand, $E_f(\pi/2)$ (in the direction of the major axis) decreases much faster than the inverse of distance near the edge of the source area, indicating that the lateral dispersion of wave energy is stronger than the ordinary geometrical spreading.

Fig. 8 shows the directivity coefficient Q at $R/A=4$, as a function of θ for the length ratios, $B/A=1$, 2 and 3. As is expected, with the

increase of B/A the variation of Q with θ increases. The minimum of Q lies somewhere around $\theta=3\pi/8$ but in the range, $\pi/4\lesssim\theta\lesssim\pi/2$, Q does not differ much from this minimum value. For the case of $B/A=1$, two local minimums of Q appear because of the symmetry of the wave form relative to the direction of $\theta=\pi/4$ but the variation of Q is, in general, very small. For $B/A=3$, the decrease of Q with θ is very rapid for small values of θ, showing a very strong directivity. The ratios $Q(\pi/2)/Q(0)$ at $R/A=4$ are 0.326 and 0.187 for $B/A=2$, and 3 respectively. The variation of Q with θ shown in Fig. 8 suggests strongly that, in practice, it is rather difficult to estimate the total energy of a tsunami from the energy flux measured at a single location unless information on the source characteristics is available.

c) Rectangular source with the combination of linear variation of deformation (Model A2)

A model considered here has sides with the lengths l_1, l_2, and l_3 whereby $l_1+l_2+l_3=2a$ and the heights are D_0 and D_0'. The bottom deformation D is limited within $|y^*|\leqslant b$ and the x^*-dependence is given by

$$D/D_0=\begin{cases}\alpha_1(x_1-x^*), & \text{for } x_2<x^*\leqslant x_1,\\ \alpha_2(x_C-x^*), & \text{for } x_3<x^*\leqslant x_2,\\ \alpha_3(x_4-x^*), & \text{for } x_4\leqslant x^*\leqslant x_3,\end{cases}\qquad(5\cdot3)$$

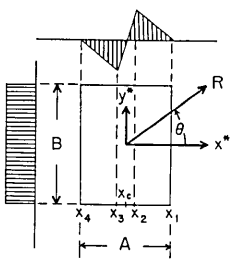

Fig. 9. Co-ordinate systems relative to the source geometry.

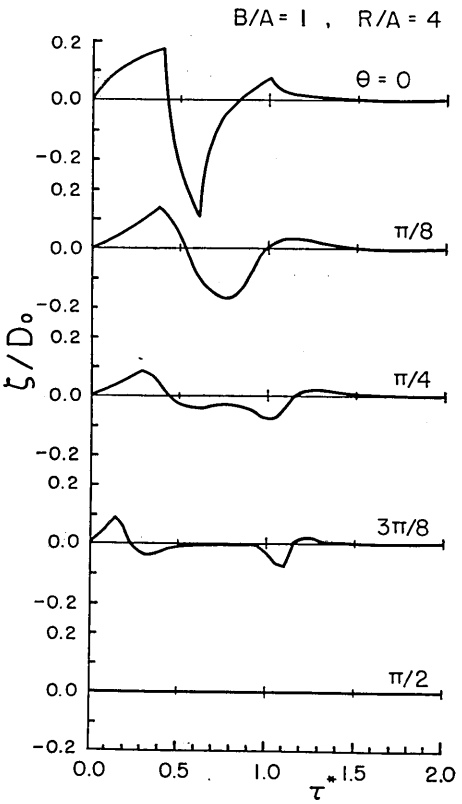

Fig. 10. Directional difference of wave forms at $R/A=4$, for Model $A2$ with $T\to0$ and $B/A=1$.

where $\alpha_1=1/l_1$, $\alpha_2=-(1+\gamma)/l_2$, $\alpha_3=\gamma/l_3$ with $\gamma=D_0'/D_0$. The other parameters are $x_1=a$, $x_2=x_1-l_1$, $x_C=x_2-l_2/(1+\gamma)$, $x_3=x_2-l_2$ and $x_4=x_3-l_3$. As an example, the case when $\gamma=1$ and $l_1=l_3=2l_2$ is shown in Fig. 9, where $A=2a$ and $B=2b$.

The computed dependence of the wave form on the direction θ is shown in Fig. 10 for $B/A=2$, and $R/A=4$. The directional difference of the wave form is quite large, reflecting the variation of the directional source function. For example, at $\theta=3\pi/8$, the wave train is divided into two groups of crests and troughs, the second one of which is quite similar to the first one but the shape is inverted. This is due to the characteristics of the given source model, for which the directional source function vanishes in the central part of the source area as θ approaches $\pi/2$.

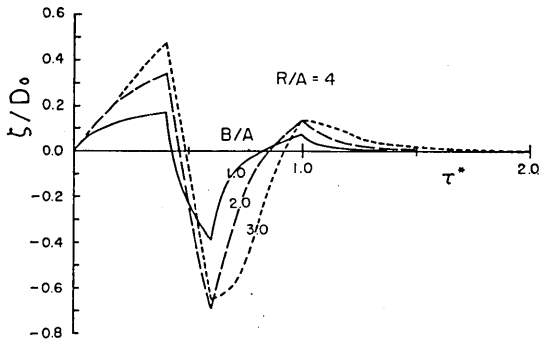

Fig. 11. Comparison of wave forms at a fixed distance $R/A=4$ in the direction of the x-axis, for Model A2 with $B/A=1$, 2, and 3.

The dependence of the wave form on the ratio B/A is shown in Fig. 11 for $\theta=0$ and $R/A=4$. It is noticed that, in general, the first crest height is smaller than the following trough depth and a small secondary crest appears after the major trough, in spite of the fact that the bottom deformation in the direction of the x^*-axis is antisymmetric with respect to the center.

For long distances from the source, the wave pattern can be computed easily by means of (2·12) (see Appendix B), and in the present example, the height ratios become 2.28 and 0.45 for trough/1st crest, and 2nd crest/1st crest, respectively.

In general, a steep scarp of the fault produces a deep trough in the generated wave at long distances from the source.

6. Asymptotic wave form for long distances from an elliptic source (Model B)

Elliptic source models are defined by:

(B1) uniform deformation; $D/D_0=1$, (6·1)

(B2) elliptic deformation; $D/D_0=\{1-(x^*/a)^2-(y^*/b)^2\}^{1/2}$, (6·2)

(B3) parabolic deformation; $D/D_0=1-(x^*/a)^2-(y^*/b)^2$, (6·3)

within the area bounded by

$$(x^*/a)^2+(y^*/b)^2=1.$$

Now take the X-axis in the direction of the observing point with the origin at the center of the source. Then the directive source function W defined by (2·11) in the direction X can be written as

$$W(X)=2b^*D_0\begin{cases}\{1-(X/a^*)^2\}^{1/2},\\ (\pi/4)\{1-(X/a^*)^2\},\\ (2/3)\{1-(X/a^*)^2\}^{3/2},\end{cases} \tag{6·4}$$

for Models B1, B2 and B3, respectively. a^* and b^* are defined by,

$$1/a^{*2}=(1-\sin^2 2\theta/2)/(a^2\cos^2\theta+b^2\sin^2\theta), \tag{6·5}$$

and

$$1/b^{*2}=\sin^2\theta/a^2+\cos^2\theta/b^2. \tag{6·6}$$

These expressions show that the directive source function is similar for all directions, provided that the parameters a^* and b^* corresponding to lengths of axes of the ellipse in the directions of X and Y are given by (6·5) and (6·6).

The wave form for long distances from the source, then, can be derived in the form (see Appendix C),

$$\zeta/D_0=(b^*/\sqrt{a^*R})\zeta^* \tag{6·7}$$

with

$$\zeta^*=\{F(t_1^*)-F(t_2^*)\}a^*/(2\pi cT), \tag{6·8}$$

and for $T\to 0$,

$$\zeta^*=G(t^*). \tag{6·9}$$

Here, t^* is defined by $\{\tau-(R-a^*)\}/a^*$ and indicates the non-dimensional time from the first arrival of disturbances at the observing point. $F(t^*)$ and $G(t^*)$ are given by simple algebraic formulas (Model B2) or by the combination of the complete elliptic integrals of the 1st and the 2nd kinds (Model B1 and B3). It may be mentioned here that the wave forms due to models similar to B1, and B3 are computed by Momoi (1962, 1963) by a completely different method, in which the high wave number components are truncated in the Fourier-Bessel expansion of the wave form.

(6·8) and (6·9) show that for large values of cT/a^*, the maximum

wave height is given by the maximum of $F(t_1^*)$ and the height varies as $b^*\sqrt{a^*/R}$ in contrast to the case when $T\to 0$, in which the maximum height varies as $b^*/\sqrt{a^*R}$. The dependence of the maximum wave height on the duration T is shown in Fig. 12, where the variation of ζ^*_{max} on cT/a^* for Model B3 is given for $b^*/a^*=2$, 3, and 4. As is expected, the decrease of ζ^*_{max} with the increase of cT/a^* is larger for larger values of b^*/a^*. If we compare the maximum wave heights in the directions of the major and the minor axes of the ellipse, the height ratio is found to decrease from $(b/a)^{3/2}$ to $(b/a)^{1/2}$ with the increase of the duration cT/a.

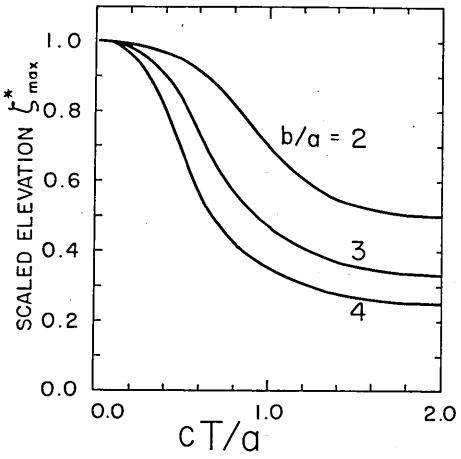

Fig. 12. Dependence of the maximum of the scaled elevation ζ^*_{max} on the duration of the bottom movement cT/a for Model B3 with $b/a=2$, 3 and 4.

For the case of the sudden deformation $T\to 0$, the total flux of wave energy in a particular direction defined by (5·1) becomes

$$E_f(\theta)=\rho g D_0^2 b^{*2}/R\int_0^\infty G^2(t^*)\,dt^*, \tag{6·10}$$

and, since the integral part is invariant with respect to the direction θ, the directivity function $R(\theta)$ defined by

$$R(\theta)=E_f(\theta)/E_f(0), \tag{6·11}$$

becomes

$$R(\theta)=(b^*/b)^2=\{\cos^2\theta+(b/a)^2\sin^2\theta\}^{-1}. \tag{6·12}$$

For $b/a=2$, 3, and 4, the dependence of $R(\theta)$ on θ is shown in Fig. 13. The minimum value is found at $\theta=\pi/2$ where $R(\pi/2)=(a/b)^2$. The general pattern of $R(\theta)$ given in Fig. 13 is comparable to the directivity coefficient $Q(\theta)$ given in Fig. 8. Both figures show that, roughly speaking, the variations are very rapid for small θ and almost constant for θ larger than $\pi/4$, in spite of the difference of the source models used.

If we imagine a straight boundary perpendicular to the x^*-axis (the direction of the minor axis of the source) at a distance x_B^* from the source center, the variation of the maximum wave height along the boundary can be expressed, by means of (6·7) and (6·9) as

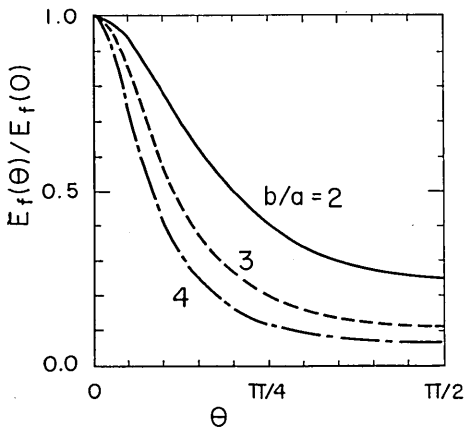

Fig. 13. Variation of the directivity function $E_f(\theta)/E_f(0)$ with the azimuth θ for Model B3 with $b/a=2$, 3, and 4.

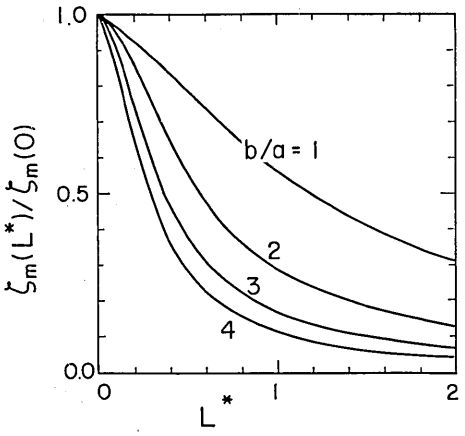

Fig. 14. Relative maximum height distribution along a straight coast perpendicular to the x^*-axis for Model B3, with $b/a=1$, 2, 3, and 4. $L^*=L/x_B^*$: L, distance along the coast, and x_B^*, shortest distance from the source center to the coast.

$$\zeta_m(L^*)/\zeta_m(0)=(x_B^*/R)^{1/2}(b^*/b)(a/a^*)^{1/2}$$
$$=[(1+L^{*2})(\sqrt{1+L^{*2}}-L^*)/\{1+(L^*b/a)^2\}^3]^{1/4}, \qquad (6\cdot13)$$

where $L^*(=y^*/x_B^*)$ is the non-dimensional distance along the boundary measured from the intersection of the x^*-axis with the boundary.

Fig. 14 shows the variation of wave heights for $B/A=1$, 2, 3, and 4. Compared with the case of $b/a=1$, which is a symmetric source model, the cases of $b/a=2$ or larger show strong directivity, and the distance L^* for which the local wave height decreases to 1/2 of the maximum height are 0.56, 0.36, 0.29 for $b/a=2$, 3, 4, respectively, in contrast to 1.19 for the symmetric case.

7. Comparison of non-dispersive and dispersive wave forms

For long distances from a source, the asymptotic wave form, taking the effect of the gravity wave dispersion into account, can be computed by the method developed in Paper I. Here, we compare the non-dispersive and dispersive wave forms for the case of an instantaneous bottom deformation of Model A1 and B3.

In both models the wave form in the x^*-direction can be expressed by

$$\zeta/D_0=(b/\sqrt{aR})\zeta^* \qquad (7\cdot1)$$

where in Model A1, $a=A/2$ and $b=B/2$. In the case of a non-dispersive wave, ζ^* is a function of t^* only defined by

$$t^*=\{\tau-(R-a)\}/a, \tag{7·2}$$

which is a non-dimensional time measured from the first arrival of non-dispersive waves at the observing point.

In the case of dispersive waves, the scaled elevation ζ^* is a function of p^* and p_a or t^* and p_a, and does not depend explicitly on R and b. The parameters p^* and p_a given in Paper I are defined in the present notations by

$$p^*=(6h/\tau)^{1/3}(R-\tau)/h=(1-t^*)p_a, \tag{7·3}$$

$$p_a=(6h/\tau)^{1/3}(a/h)\simeq(6h/R)^{1/3}(a/h). \tag{7·4}$$

The last expression of (7·4) holds if we confine our attention to the main part of the wave train only $(a(1-t^*)/(3R)\ll 1)$. The formula to compute ζ^* for Model A1 and Model B3 can be derived from (94) and (98) in Paper I, respectively, by a slight modification.

Thus, we may write

$$\zeta^*=\left(\frac{p_a^{1/2}}{\pi^{3/2}}\right)\begin{cases} T(p^*-p_a)-T(p^*+p_a), & \text{for Model A1,} \\ 2\int_{-1}^{1} T(p^*-\alpha p_a)\alpha\sqrt{1-\alpha^2}\,d\alpha, & \text{for Model B3,} \end{cases} \tag{7·5}$$

where $T(p)$ is defined by

$$T(p)=Re\left[(1+i)\int_0^\infty \exp i(u^6+pu^2)\,du\right] \tag{7·6}$$

and is shown in Fig. 3a of Paper I.

In Fig. 15a, b, the dispersive and non-dispersive wave forms ζ^* are compared for Model A1 and Model B3, respectively. It is easily seen that Model A1 contains more energy in high wave number components than Model B3, so that the difference of the dispersive and non-dispersive wave forms is greater in Model A1 than in Model B3 for the same parameter p_a.

It is remarkable that, for Model B3, two wave forms for the dispersive and non-dispersive cases are relatively similar up to about $p_a\sim 4$. This indicates that the non-dispersive assumption is satisfactory for large values of p_a, but for $p_a=2$, for example, the wave forms are different, showing the significance of dispersion. For Model A1, dispersive waves of high frequencies appear from the beginning, but the non-dispersive wave forms represents a kind of smoothed version of dispersive waves for large values of p_a.

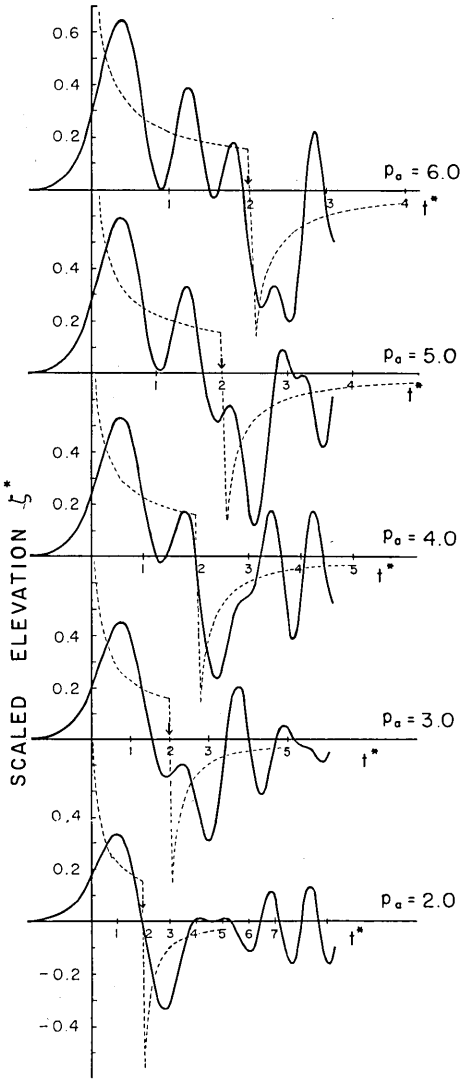

Fig. 15a. Comparison of the scaled wave forms ζ^* for Model A1 in the x^*-direction for the non-dispersive (- - -), and dispersive (——) cases. An arrow indicates the time when the disturbance from the rear end of the source arrives at the observing point with the velocity c.

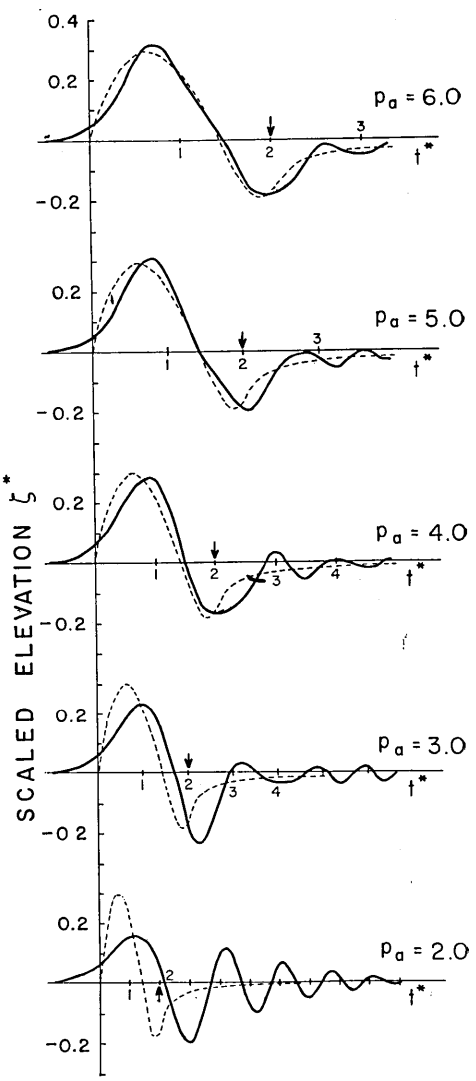

Fig. 15b. Comparison of the scaled wave forms ζ^* for Model B3 in the x^*-direction for the non-dispersive (- - -) and dispersive (——) cases.

To see the applicability of the non-dispersive assumption which may be limited by the condition $p_a \gtrsim 4$, a diagram is constructed in Fig. 16, where the relations between R/h, a/h and p_a are shown. The assumption of long distances requires the condition $a/R \lesssim 0.1$, and the scale of

the ocean is delineated by assuming $R=20,000\,Km$ and $h=4\,Km$. From this diagram, it is found that if $a/h=20$ or $a=80$ Km, the non-dispersive assumption for Model B is satisfactory up to $R/h\sim800$, or $R\sim3200\,Km$ and the minimum value of p_a is about 2. On the other hand, if $a/h=5$ or $a=20\,Km$, the same limiting distance becomes $R\sim50\,Km$ and the assumption of a long distance is invalidated. The actual scale of the tsunami source L is somewhere around several tens Km to several hundred Km at the depth of $2\sim3\,Km$. To convert the scale L at depth h_0 to the scale a at depth h, we should apply the relation $a=\sqrt{h/h_0}(L/2)$.

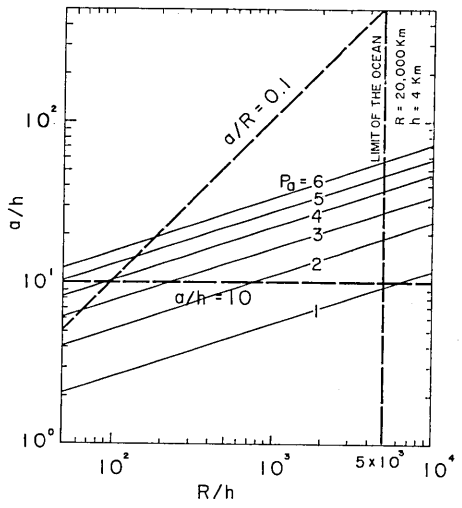

Fig. 16. Diagram indicating the range of the validity of the non-dispersive assumption as a function of a/h and R/h.

Fig. 16 indicates that, if the tsunami propagation is to be discussed, the long-wave equation can be used near the wave source of large horizontal extent, i.e., for tsunamis generated by near earthquakes in the vicinity of the Japanese coast, but it is not a good approximation for the tsunami propagation in the whole Pacific Ocean.

8. Concluding remarks

In the present paper, the following topics are discussed for a sea of constant depth: 1) the energy exchange between the solid bottom and the overlying water associated with the broad crustal deformation —in particular, the dependence of energy exchange on the duration of the bottom movement, 2) the variations of wave forms in two-dimensional propagation and the directivity of energy radiation, 3) the effect of the gravity wave dispersion.

Most of the conclusions obtained are rather sensitive to the assumed source characteristics and we should be careful when generalizing. This, in turn, suggests that the estimation of the source characteristics is essential to the prediction of a tsunami wave form.

To develop a method to solve the inverse problem, various factors not included in the present paper should be examined. One of the important first step seems to be the evaluation of the effects of the

bottom topography near the tsunami source—the directivity of energy radiation would be modified significantly. The deep water tsunami signatures is expected to include the effects of multiple reflections on the continental shelf near the source and this problem will be discussed in a separate paper.

To obtain wave forms under conditions of a realistic topography and source, it is necessary to resort to a hydrodynamical-numerical method, where the starting equations of motion should be selected in relation to the scales of the source and the ocean area concerned. The inverse problem would then be solved by comparing wave forms computed on various probable source models with observations.

Acknowledgments

The author is grateful to Miss Ikuko Kato for various technical assistance.

References

AIDA, I., 1969, Numerical experiments for the tsunami propagation—the 1964 Niigata tsunami and the 1968 Tokachi-oki tsunami, *Bull. Earthq. Res. Inst.*, **47**, 673-700.

HATORI, T., 1963, Directivity of tsunamis, *Bull. Earthq. Res. Inst.*, **41**, 61-81.

IIDA, K., 1966, The Niigata tsunami of June 16, 1964, *General Report on the Niigata Earthquake of 1964*, Pt. 1-6, 97-127, Tokyo Electrical Eng'ng College Press.

KAJIURA, K., 1963, The leading wave of a tsunami, *Bull. Earthq. Res. Inst.*, **41**, 535-571.

MIKUMO, T., 1968, Atmospheric pressure waves and tectonic deformation associated with the Alaskan Earthquake of March 28, 1964, *J. Geophys. Res.*, **73** (6), 2009-2025.

MIYOSHI, H., 1954, Generation of the tsunami in compressible water, Part 1, *J. Oceanogr. Soc. Japan*, **10**, 1-9.

MIYOSHI, H., 1954, Efficiency of the tsunami, *J. Oceanogr. Soc. Japan*, **10**, 11-14.

MIYOSHI, H., 1955, Directivity of the recent tsunamis, *J. Oceanogr. Soc. Japan*, **11**(4), 151-156.

MIYOSHI, H., 1968, Re-consideration on directivity of the tsunami (1) (in Japanese), *Zisin*, **ii**, **21**, 121-138.

MOMOI, T., 1962, The directivity of tsunami (1): the case of instantaneously and uniformly elevated elliptic wave origin, *Bull. Earthq. Res. Inst.*, **40**, 297-307.

MOMOI, T., 1963, Some remarks on generation of waves from elliptical wave origin, *Bull. Earthq. Res. Inst.*, **41**, 1-8.

SOLOVIEV, S. L., 1965, The Urup earthquake and associated tsunami of 1963, *Bull. Earthq. Res. Inst.*, **43**, 103-109.

SOLOVIEV, S. L., 1969, On recurrence of tsunamis in the Pacific, *IUGG Tsunami Symposium Hawaii, 1969*, Hawaii Univ. Press.

TAKAHASI, R., 1942, On seismic sea waves caused by deformations of the sea bottom (in Japanese), *Bull. Earthq. Res. Inst.*, **20**, 375-400.

TAKAHASI, R. and HATORI, T., 1962, A model experiment on the tsunami generation from a bottom deformation area of elliptic shape (in Japanese), *Bull. Earthq. Res. Inst.*, **40**, 873-883.

Appendix A Wave in a one-dimensional model

The Green's function for one-dimensional wave propagation is given by

$$G(x, t \mid x_0, t_0)=2c\pi\{1-H[|x-x_0|/c-(t-t_0)]\}, \tag{A·1}$$

where x and x_0 are horizontal co-ordinates of the observing point and the source, respectively. Taking the time origin at the beginning of the bottom movement, we have the movement in $0\leqslant t_0\leqslant T$.

For the uniform deformation D_0 of the bottom in the generating area delineated by $a\geqslant x_0\geqslant -b$, the elevation $\zeta(x, t)$ is given by

$$\zeta/D_0=1/(4\pi c^2T)\int_{-b}^{a}\{G(x, t \mid x_0, 0)-G(x, t \mid x_0, T)\}dx_0. \tag{A·2}$$

The integration of (A·2) is straight forwards and if x is inside the source region,

$$\zeta/D_0=1/(2T)\left[\begin{pmatrix}ct\\a\end{pmatrix}+\begin{pmatrix}ct\\b\end{pmatrix}\right]_{t_0=T}^{t_0=0}, \tag{A·3}$$

and if x is outside the source region $(x>a)$,

$$\zeta/D_0=1/(2T)\left[\begin{pmatrix}ct'\\A\end{pmatrix}\right]_{t_0=T}^{t_0=0}, \tag{A·4}$$

where $ct'=ct-(x-a)$, and $A=a+b$. Here the following abbreviation is adopted:

$$\begin{pmatrix}ct\\a\end{pmatrix}=\begin{cases}ct, & \text{for } ct\leqslant a,\\ a, & \text{for } ct>a,\end{cases}$$

and

$$[F]_{t_0=T}^{t_0=0}=F(t_0=0)-F(t_0=T).$$

Now if the observing point is at the origin of the co-ordinate which is inside the source region and $t<T$, we have

$$\zeta/D_0=1/(2T)\begin{cases}2ct, & \text{for } ct\leqslant a,\\ a+ct, & \text{for } a<ct\leqslant b,\\ A, & \text{for } b<ct\leqslant cT.\end{cases} \tag{A·5}$$

Therefore, the energy e transferred by the bottom deformation to the gravity wave at the origin is given by

$$e=\rho g D_0/T\int_0^T \zeta dt$$
$$=(1/2)\rho g D_0^2\begin{cases}1, & \text{for } cT\leqslant a\\ 1/(2T^2)\{T^2+2aT/c-(a/c)^2\}, & \text{for } a/c<T\leqslant b/c,\\ 1/(2T^2)\{2AT/c-(a/c)^2-(b/c)^2\}, & \text{for } T>b/c.\end{cases} \quad (A\cdot 6)$$

Integrating this energy for the whole source region with the length A, we have

$$E_D/E_{D0}=\begin{cases}1-cT/(3A), & \text{for } cT\leqslant A,\\ A^2/(cT)^2(cT/A-1/3), & \text{for } cT>A,\end{cases} \quad (A\cdot 7)$$

where

$$E_{D0}=(1/2)\rho g D_0^2 \mathrm{A}. \quad (A\cdot 8)$$

Appendix B Asymptotic solutions for long distances from a rectangular sources

For long distances from a source, wave forms can be computed from (2·10) or (2·11), which are written in terms of rectangular co-ordinate system (x, y) with the origin at the observing point and the x-axis directed to the center of the source area. However, to compute the directive source function, it is convenient to take right-handed rectangular co-ordinates (x^*, y^*) and (X, Y) with the origin at the center of a source. The x^*-axis is taken parallel to an edge of the rectangle, and the X-axis is directed toward the observing point. The azimuth of the X-axis relative to the x^*-axis is θ and the distance to the observing point from the origin is R.

(a) Rectangular uniform source (Model A1)

If the uniform uplift of the bottom occurs in a rectangular area;

$$D/D_0=1, \quad \text{for} \quad |x^*|\leqslant a, \quad \text{and} \quad |y^*|\leqslant b, \quad (B\cdot 1)$$

the directive source function W defined by (2·11) can be given, by projecting the corners of the source area on the X-axis, as follows:

$$W(X)=2b^*D_0\begin{cases}(a^*-X)/\Delta, & \text{for } a^{**}<X\leqslant a^*,\\ 1, & \text{for } -a^{**}\leqslant X\leqslant a^{**},\\ (a^*+X)/\Delta, & \text{for } -a^*\leqslant X<-a^{**}.\end{cases} \quad (B\cdot 2)$$

Here, from the geometry of a rectangle relative to the (X, Y) co-ordinates, we have

$$a^*=a\cos\theta+b\sin\theta, \tag{B·3}$$

$$a^{**}=|\,a\cos\theta-b\sin\theta\,|, \tag{B·4}$$

$$\Delta=a^*-a^{**} \tag{B·5}$$

and

$$b^*=\begin{cases} b/\cos\theta, & \text{for} \quad 0\leqslant\theta\leqslant\theta^*, \\ a/\sin\theta, & \text{for} \quad \theta^*\leqslant\theta\leqslant\pi/2, \end{cases} \tag{B·6}$$

with $\tan\theta^*=b/a$.

The solution for η given by (2·10) is now transformed to

$$\eta/D_0=(4\sqrt{2}/3)\sqrt{a^*/R}(b^*/\Delta')\{\xi_s^{3/2}H(\xi_s) - (\xi_s-\Delta')^{3/2}H(\xi_s-\Delta')-(\xi_e+\Delta')^{3/2}H(\xi_e+\Delta')+\xi_e^{3/2}H(\xi_e)\} \tag{B·7}$$

where $\Delta/a^*=\Delta'$ and

$$\xi_s=\{\tau-(R-a^*)\}/a^*, \quad \xi_e=\{\tau-(R+a^*)\}/a^*. \tag{B·8}$$

For a limiting case of $\Delta'\to 0$, we have

$$\eta/D_0=2\sqrt{2}\sqrt{a^*/R}\,b^*\{\xi_s^{1/2}H(\xi_s)-\xi_e^{1/2}H(\xi_e)\}, \tag{B·9}$$

where $\Delta'\to 0$ corresponds to the situation when $\theta=0$ or $\pi/2$, and $b^*=b$ or a, respectively.

For an instantaneous deformation ($T\to 0$), (2·11) gives, in terms of ξ

$$\zeta/D_0=(\sqrt{2}/\pi)b^*/(\Delta'\sqrt{Ra^*})\{\xi_s^{1/2}H(\xi_s)-(\xi_s-\Delta')^{1/2}H(\xi_s-\Delta') - (\xi_e+\Delta')^{1/2}H(\xi_e+\Delta')+\xi_e^{1/2}H(\xi_e)\}, \tag{B·10}$$

and for a limiting case of $\Delta'\to 0$,

$$\zeta/D_0=1/(\sqrt{2}\pi)(b^*/\sqrt{Ra^*})\{\xi_s^{-1/2}H(\xi_s)-\xi_e^{-1/2}H(\xi_e)\}. \tag{B·11}$$

(B·11) shows that ζ/D_0 becomes infinite for $\xi_s\to 0$ or $\xi_e\to 0$. This is due to the deficiency of the directive source function $W(x)$ near the edge of the source as already mentioned in Section 2. In the interval, $0\leqslant\xi_s\leqslant\varepsilon$ or $-\varepsilon\leqslant\xi_e\leqslant 0$ with $\varepsilon\sim b^2/(2R)$, we should return to the exact formula. For example, in the interval $0\leqslant\xi_s\leqslant\varepsilon$, we have

$$\eta/D_0=\pi\tau H(\xi_s), \quad \text{and for} \quad T\to 0, \ \zeta/D_0=1/2H(\xi_s). \tag{B·12}$$

Since the elevation ζ for a duration cT is given by substituting (B·9) into (2·5) with an appropriate change of ξ_s and ξ_e, it is found that the elevation for $\Delta=0$ with the duration cT is similar to the elevation from the instantaneous deformation if Δ is put equal to cT and b^* is equal to b or a in (B·10).

(b) **Rectangular source with linear variation of deformation (Model A2)**

A model defined by (5·3) can be transformed to

$$D/D_0=\sum_{i=1}^{4}\beta_i(x_i-x^*)H(x_i-x^*)\,, \tag{B·13}$$

where

$$\beta_1=\alpha_1,\ \ \beta_2=(\alpha_2-\alpha_1),\ \ \beta_3=(\alpha_3-\alpha_2)\ \text{ and }\ \beta_4=-\alpha_3.$$

In this formulation, the contribution from, say, the first term in (B·13) to the directive source function $W(X)$ in the direction X can be written as

$$W(X)=\int_{Y_1}^{Y_2}Dd\,Y=D_0\beta_1(Y_2-Y_1)\{(x_1-X\cos\theta)+(1/2)\sin\theta(Y_2+Y_1)\} \tag{B·14}$$

where

$$\begin{aligned} Y_2&=b/\cos\theta-X\tan\theta,\quad \text{for}\quad X_1\geqslant X,\\ Y_1&=\begin{cases} X/\tan\theta-x_1/\sin\theta, & \text{for}\quad X_1\geqslant X\geqslant X_1^*,\\ -b/\cos\theta-X\tan\theta, & \text{for}\quad X_1^*\geqslant X,\end{cases}\end{aligned} \tag{B·15}$$

and

$$\begin{aligned} X_1&=x_1\cos\theta+b\sin\theta,\\ X_1^*&=x_1\cos\theta-b\sin\theta.\end{aligned} \tag{B·16}$$

Therefore, it follows:

$$\begin{aligned} W(X)=&D_0\beta_1/(2\sin\theta\cos^2\theta)\\ &\times\begin{cases}(X_1-X)^2, & \text{for}\quad X_1\geqslant X\geqslant X_1^*,\\ 4b\sin\theta(x_1\cos\theta-X), & \text{for}\quad X_1^*>X,\end{cases}\end{aligned} \tag{B·17}$$

and

$$\begin{aligned} -\partial W/\partial X=&D_0\beta_1/(\sin\theta\cos^2\theta)\\ &\times\begin{cases}(X_1-X), & \text{for}\quad X_1\geqslant X\geqslant X_1^*,\\ 2b\sin\theta, & \text{for}\quad X_1^*>X.\end{cases}\end{aligned} \tag{B·18}$$

Thus, the surface elevation for the case of an instantaneous deformation ($T\to 0$) is given by

$$\zeta/D_0=1/(2\pi\sqrt{2R}\sin\theta\cos^2\theta)\sum_{i=1}^{4}\beta_i I_i\,, \tag{B·19}$$

where

$$I_i=2[t_i\sqrt{\xi}-\xi^{3/2}/3]_{t_i^*}^{t_i}+4b\sin\theta\sqrt{t_i^*}, \tag{B·20}$$

and

$$t_i=\tau-(R-X_i),\quad t_i^*=\tau-(R-X_i^*). \tag{B·21}$$

The expression I_i holds provided that t_i and t_i^* are positive. In explicit form, we have

$$I_i=\begin{cases}(4/3)t_i^{3/2}, & \text{for } t_i>0 \text{ and } t_i^*\leqslant 0,\\ (2/3)(b\sin\theta)\{2t_i/(\sqrt{t_i}+\sqrt{t_i^*})+5\sqrt{t_i^*}\}, & \text{for } t_i^*>0.\end{cases} \tag{B·22}$$

In particular, for the wave propagating in the x^*-direction ($\theta=0$), in which $X_i=X_i^*$ and $t_i=t_i^*$, (B·19) becomes

$$\zeta/D_0=(1/\pi)\sqrt{2/R}\,b\sum_{i=1}^{4}\beta_i\sqrt{t_i}\,H(t_i), \tag{B·23}$$

and the first crest ζ_c and the following trough ζ_t occur at $t_2=0$ and $t_3=0$, respectively. Furthermore, the second crest appears at $t_4=0$. Therefore, we have,

$$|\,\zeta_t/\zeta_c\,|=|\,\sqrt{1+l_2/l_1}+(\beta_2/\beta_1)\sqrt{l_2/l_1}\,|. \tag{B·24}$$

It is easy to derive the ratio of the heights of the second crest ζ_c' to the first crest ζ_c in the similar way. Thus,

$$\zeta_c'/\zeta_c=(\beta_1\sqrt{l_1+l_2+l_3}+\beta_2\sqrt{l_2+l_3}+\beta_3\sqrt{l_3})/(\beta_1\sqrt{l_1}). \tag{B·25}$$

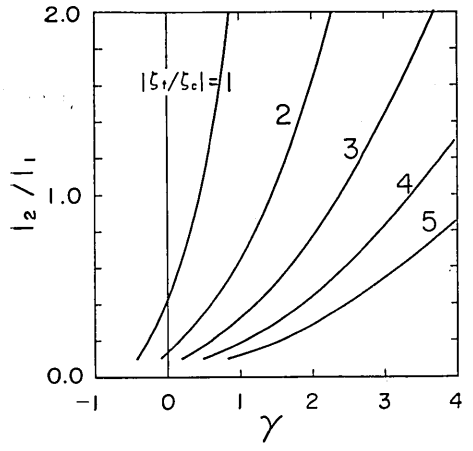

Fig. B-1. Relation between l_2/l_1 and γ with ζ_t/ζ_c as a parameter.

If we go back to the original parameters defined in (5·3), it follows

$$\beta_2/\beta_1=-\{1+(1+\gamma)l_1/l_2\}. \tag{B·26}$$

The relation between l_2/l_1 and γ with $|\,\zeta_t/\zeta_c\,|$ as a parameter is shown in Fig. B·1, from which we can estimate the height ratio for given values of l_2/l_1 and γ. For example, $|\,\zeta_t/\zeta_c\,|=2.28$ for $\gamma=1$ and $l_2/l_1=0.5$ which is an example given in Section 5-c. For this example, $\zeta_c'/\zeta_c=0.45$ from (B·25).

Appendix C Elliptic source models

Let us transform the variables by putting

$$\lambda^2=(\tau-x)/a^*, \quad \alpha^2=\{\tau-(R-a^*)\}/a^*, \tag{C·1}$$

and

$$\beta^2=\{\tau-(R+a^*)\}/a^*,$$

where x is the co-ordinate with the origin at the observing point. Then, it follows:

$$(\alpha^2-\beta^2)=2,$$

$$dx/\sqrt{\tau-x}=-2\sqrt{a^*}d\lambda,$$

and

$$X/a^*=1-(\alpha^2-\lambda^2)=(\lambda^2-\beta^2)-1.$$

The directive source functions (6·4) can be written as

$$\mathrm{W}(x)=2b^*D_0f(\lambda), \tag{C·2}$$

with

$$f(\lambda)=\begin{cases}\{(\alpha^2-\lambda^2)(\lambda^2-\beta^2)\}^{1/2},\\ (\pi/4)(\alpha^2-\lambda^2)(\lambda^2-\beta^2),\\ (2/3)\{(\alpha^2-\lambda^2)(\lambda^2-\beta^2)\}^{3/2},\end{cases} \tag{C·3}$$

and

$$dW(x)/dx=(2b^*D_0/a^*)g(\lambda), \tag{C·4}$$

with

$$g(\lambda)=\begin{cases}\{1-(\alpha^2-\lambda^2)\}\{(\alpha^2-\lambda^2)(\lambda^2-\beta^2)\}^{-1/2}\\ (\pi/2)\{1-(\alpha^2-\lambda^2)\},\\ 2\{1-(\alpha^2-\lambda^2)\}\{(\alpha^2-\lambda^2)(\lambda^2-\beta^2)\}^{1/2}.\end{cases} \tag{C·5}$$

Substituting these relations into (2·10) or (2·11), we have the solution of the form:

$$\eta/\mathrm{D}_0=2\sqrt{2}\,b^*\sqrt{a^*/R}\int_\beta^\alpha f(\lambda)H(\lambda)d\lambda, \tag{C·6}$$

and for $T\to 0$,

$$\zeta/D_0=(\sqrt{2}/\pi)(b^*/\sqrt{a^*R})\int_\beta^\alpha g(\lambda)H(\lambda)d\lambda. \tag{C·7}$$

It is remarked that for $\tau<R+a^*$, β^2 is negative and the lower limit of the integration in (C·6) and (C·7) should be put zero.

The integrals in (C·6) and (C·7) are composed essentially of the following kind of integrals:

$$I_{l,m}=\int_0^\alpha(\alpha^2-\lambda^2)^{l/2}(\lambda^2+|\beta|^2)^{m/2}d\lambda, \quad \text{for} \quad \beta^2\leqslant 0, \tag{C·8a}$$

and

$$J_{l,m}=\int_\beta^\alpha(\alpha^2-\lambda^2)^{l/2}(\lambda^2-\beta^2)^{m/2}d\lambda, \quad \text{for} \quad \beta^2>0. \tag{C·8b}$$

If both l and m are 0 or even numbers, the integration can be performed without difficulty. The solution for Model B2 corresponds to this case. On the other hand, if l and m are odd numbers, the solution is given in terms of the complete elliptic integrals.

Now, (C·8a) is transformed, by putting $\lambda=\alpha\sin\theta$ into

$$I_{l,m}=\{(\alpha^2+|\beta^2|)^{m/2}\alpha^{l+1}\}\int_0^{\pi/2}\cos^{(l+1)}\theta(1-k^2\cos^2\theta)^{m/2}d\theta, \tag{C·9}$$

where

$$k^2=\alpha^2/(\alpha^2+|\beta^2|),$$

and (C·8b) is transformed by putting $\lambda^2=\alpha^2\sin^2\theta+\beta^2\cos^2\theta$, into

$$J_{l,m}=\{(\alpha^2-\beta^2\}^{1+(l+m)/2}/\alpha\}\int_0^{\pi/2}\sin^{m+1}\theta\cos^{l+1}\theta/\sqrt{1-k'^2\cos^2\theta}d\theta,$$

where

$$k'^2=(\alpha^2-\beta^2)/\alpha^2. \tag{C·10}$$

(C·9) and (C·10) can be integrated by making use of the following recurrence formulas:

$$\begin{aligned}E_{2n}(k^2)&=\int_0^{\pi/2}\cos^{2n}\theta\sqrt{1-k^2\cos^2\theta}\,d\theta\\&=\{(1-k^2)K_{2n}(k^2)+(2n-1)E_{2(n-1)}(k^2)\}/(2n+1),\end{aligned} \tag{C·11}$$

and

$$\begin{aligned}K_{2n}(k^2)&=\int_0^{\pi/2}\cos^{2n}\theta/\sqrt{1-k^2\cos^2\theta}\,d\theta\\&=\{K_{2(n-1)}(k^2)-E_{2(n-1)}(k^2)\}/k^2,\end{aligned} \tag{C·12}$$

where $K_0(k^2)$ and $E_0(k^2)$ are complete elliptic integrals of the first and the second kind, respectively.

Performing the integration, the final form for (C·6) becomes,

$$\eta/D_0=b^*\sqrt{a^*/R}F(t^*). \tag{C·13}$$

The explicit form of $F(t^*)$ is as follows:

Model B1;

$$F(t^*)=8\begin{cases}k^2E_2(k^2), & \text{for } t^*\leqslant 2,\\ k'\{K_2(k'^2)-K_4(k'^2)\}, & \text{for } t^*>2,\end{cases} \tag{C·14}$$

Model B2;

$$F(t^*)=(\sqrt{2}\,\pi/3)\begin{cases}2t^{*3/2}(1-2t^*/5), & \text{for } t^*\leqslant 2,\\ t^{*3/2}(t^*/5-t^{**})-t^{**3/2}(t^{**}/5-t^*), & \text{for } t^*>2,\end{cases} \tag{C·15}$$

Model B3;

$$F(t^*)=(64/3)\begin{cases}k^4\{E_4(k^2)-k^2E_6(k^2)\}, & \text{for } t^*\leqslant 2,\\ (3/k')\{2E_6(k'^2)-3E_4(k'^2)+E_2(k'^2)\}, & \text{for } t^*>2,\end{cases} \tag{C·16}$$

with

$$k^2=t^*/2,\quad k'^2=2/t^*,\quad t^{**}=t^*-2,$$

and

$$t^*=\alpha^2=\{\tau-(R-a^*)\}/a^*.$$

$E_2(k^2)$, $E_4(k^2)$, $E_6(k^2)$, $K_2(k'^2)$, $K_4(k'^2)$ are given by (C·11) and (C·12).

In the same way, (C·7) becomes

$$\zeta/D_0=(b^*/\sqrt{a^*R})G(t^*). \tag{C·17}$$

The explicit form of $G(t^*)$ is as follows:

Model B1;

$$G(t^*)=(1/\pi)\begin{cases}\{K_0(k^2)-2k^2K_2(k^2)\}, & \text{for } t^*\leqslant 2,\\ k'\{K_0(k'^2)-2K_2(k'^2)\}, & \text{for } t^*>2,\end{cases} \tag{C·18}$$

Model B2;

$$G(t^*)=(\sqrt{2}/3)\begin{cases}\sqrt{t^*}(3/2-t^*), & \text{for } t^*\leqslant 2,\\ \sqrt{t^*}\,(3/2-t^*)+\sqrt{t^{**}}(3/2+t^{**}), & \text{for } t^*>2,\end{cases} \tag{C·19}$$

Model B3;

$$G(t^*)=(8/\pi)\begin{cases}k^2\{E_2(k^2)-2k^2E_4(k^2)\}, & \text{for } t^*\leqslant 2,\\ (2/k')[(k'^2/2-1)\{K_2(k'^2)-K_4(k'^2)\}\\ \qquad +\{E_2(k'^2)-E_4(k'^2)\}], & \text{for } t^*>2.\end{cases} \tag{C·20}$$

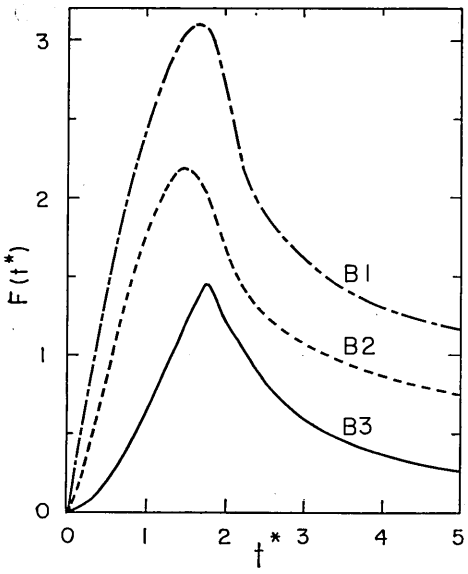

Fig. C-1. $F(t^*)$ as a function of t^* for Model B1, B2, and B3.

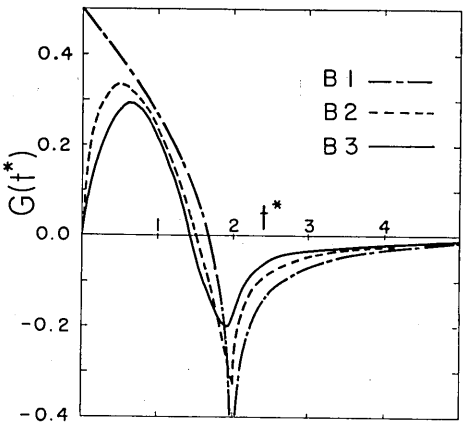

Fig. C-2. $G(t^*)$ as a function of t^* for Model B1, B2, and B3.

The time dependence of $F(t^*)$ and $G(t^*)$ for Model B1, B2, B3 are shown in Fig. C·1 and Fig. C·2, respectively. Fig. C·2 shows that the maximum height appears earlier than the time corresponding to the wave travelling from the center of the source, but the lowest level (trough) appears very close to the wave corresponding to the rear end of the source ($t^* \sim 2$). It is noticed that for Model B3, the crest height is larger than the trough depth, and for Model B2, they are equal. In particular, for Model B1, the maximum height appears at the front of the wave, and a depression of infinite amount occurs at the time corresponding to the rear end of the source. This behavior, however, is somewhat fictituous in view of an unsatisfactory approximation of the directive source function near these points.

45. 波源特性と津波エネルギー及び指向性

地震研究所 梶浦欣二郎

長波近似をもちい，海底での大規模な地殻変動によって一様水深の海で発生する津波の波形を求める式を提出し，それを用いて，(1) 地殻変動によって海水に伝えられるエネルギーが，変動継続時間によってどう変るか，(2) 津波の2次元伝播による波形変化，及びエネルギー伝播の方向性，(3) 津波伝播における重力波分散の影響，を調べた．

(1) については，継続時間が数分程度までなら，津波発生に関するかぎり，変動が瞬間的におこったとみなしてよいが，継続時間が実際に数秒程度であるとすれば，海中の圧縮性の波になるエネルギーの割合が津波のエネルギーより大きくなる可能性がある．

(2) については，簡単な矩形波源から出る津波の距離による波形変化，波形の伝播方向による違い，及びエネルギーの指向性を計算した．指向性係数の大きな変化は，波源の短軸から約45度以内の方向にかぎられる．また，波源の近傍(波源の大きさの程度)での波動エネルギーの距離による減衰は，長軸および短軸方向で著しく異なり，前者では単なる点源からの2次元的伝播による減衰より減衰が大きく，回折の影響が大きいことを示し，一方後者では減衰が小さく1次元的伝播に似てくる．楕円状の波源から遠方の点でのエネルギー伝播の方向性は，観測点と波源中心とを結ぶ方向に対して直角方向の波源のひろがり(横のスケール)の2乗に比例する．

(3) については，同一の波源から出る分散性の波と，長波近似による非分散性の波の波形を比較し，$p_a \gtrsim 4$ 程度では長波近似が有効であることが示される．ここで p_a は波源のスケール a，水深 h，波源からの距離 R によってきまるパラメータである．